ACS OMEGA

http://pubs.acs.org/journal/acsodf

Article

Electrochemiluminescence Immunosensor Based on Nanobody and Au/$CaCO_3$ Synthesized Using Waste Eggshells for Ultrasensitive Detection of Ochratoxin A

Linzhi Li,[⊥] Xing Liu,[⊥] Saijun He, Hongmei Cao,* Benchao Su, Tianzeng Huang, Qi Chen, Minghuan Liu, and Da-Peng Yang*

Cite This: *ACS Omega* 2021, 6, 30148−30156

Read Online

ACCESS | Metrics & More | Article Recommendations | Supporting Information

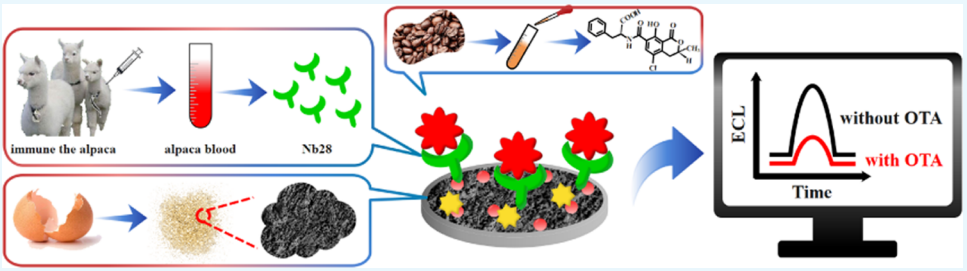

ABSTRACT: A novel ultrasensitive electrochemiluminescence (ECL) immunoassay based on Au/$CaCO_3$ was proposed for detecting ochratoxin A (OTA) in coffee. Au/$CaCO_3$ nanocomposites synthesized using waste eggshells as the template with a large surface area and excellent electrochemical properties were applied for immobilizing a large amount of $Ru(bpy)_3^{2+}$ and conjugating a high-affinity nanobody (prepared by the phage display technique). Coupling of the Au/$CaCO_3$ nanocomposites and nanobody technologies provided an ultrasensitive and highly selective ECL immunosensor for OTA detection in the range of 10 pg/mL−100 ng/mL with a low detection limit of 5.7 pg/mL. Moreover, the as-prepared ECL immunosensor showed excellent performance and high stability. Finally, the proposed ECL sensor was applied to analyze OTA in coffee samples, confirming the desirable accuracy and practical applicability potential. Overall, this work presents a new nanomaterial for fabricating the sensing interface of immunosensors by harnessing natural waste as the source and a method for detecting toxic OTA in foods.

1. INTRODUCTION

As a toxic secondary metabolite, ochratoxin A (OTA) is mainly produced by *Penicillium* and *Aspergillus* and is widely distributed in nature. It easily contaminates various food products, for instance, cereals, coffee beans, dried fruits, and spices around the world. Moreover, once OTA enters the food chain, it is quite difficult to remove due to its high thermal and chemical stabilities.[1] Numerous research studies have shown that OTA has diverse toxicities, including strong hepatotoxicity, renal toxicity, and carcinogenic and teratogenic effects, posing a serious threat to humans and animals. Therefore, International Agency for Research on Cancer (IARC) has classified OTA as a human 2B carcinogen because of its potential toxicity. To reduce the risk of OTA intake from food products, many countries and organizations have established strict maximum limits for OTA in different kinds of food, such as 5 μg/kg of raw cereal, 3 μg/kg of cereal-derived products, and 10 μg/kg of soluble coffee (European Commission).[2]

To date, various analytical methods and strategies have been developed for the detection of OTA to minimize the risk of its consumption, including thin-layer chromatography (TLC),[3] high-performance liquid chromatography (HPLC),[4] gas chromatography (GC)[5] coupled with ultraviolet−visible spectrometry, mass spectrometry (MS),[6] and enzyme-linked immunosorbent assay (ELISA).[7] Although these techniques exhibit excellent sensitivities and specificity, they suffer from some shortcomings, such as expensive instrumentation, high level of operator expertise, time-consuming sample pretreatment, and so on. Thus, it is desirable to develop other simple, rapid, and low-cost detection techniques for sensitive OTA detection. However, electrochemiluminescence (ECL) possesses unique advantages for the detection of OTA due to its low cost, rapidity, high sensitivity, low background noise, simple instrumentation, and controlled reaction system.[8,9] Wang *et al.* reported that a solid-state ECL sensor of RuSi nanoparticles for the detection of OTA was based on a molecularly imprinted polymer.[8,9] In the study, $Ru(bpy)_3^{2+}$-

Received: September 20, 2021
Accepted: October 13, 2021
Published: October 28, 2021

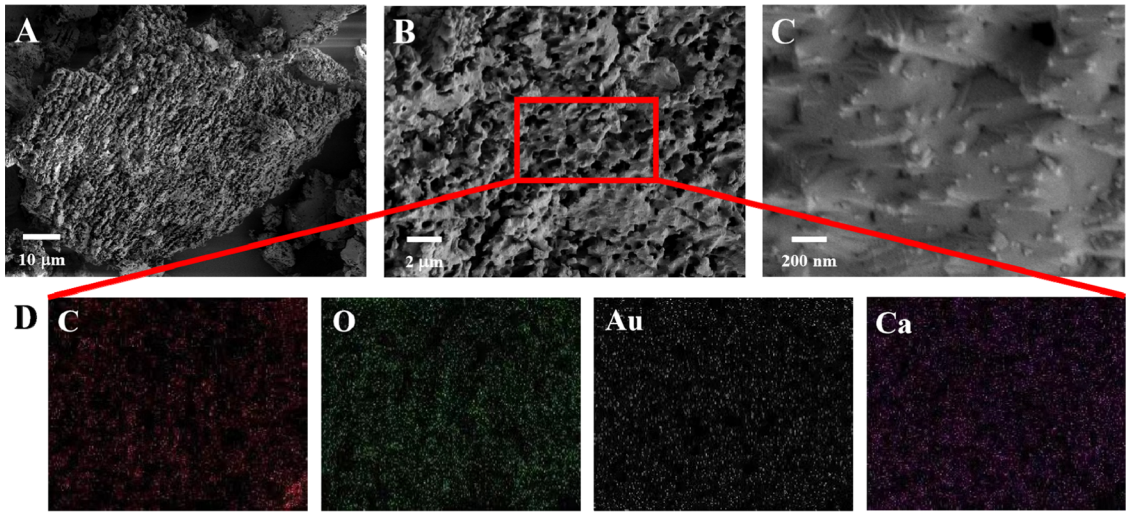

Figure 1. SEM images of $Au/CaCO_3$ (A−C) under different magnifications and the corresponding EDS elemental mapping images of C, O, Au, and Ca (D).

doped silica nanoparticles (RuSi-NPs) acted as an ECL material and the molecularly imprinted polymer as a recognizing element to capture OTA, improving the selectivity of the ECL sensor. However, the ECL immunoassay combining the superiority of ECL with the specificity of immunoreactions has gradually become a significant and powerful analytical approach in the fields of pharmaceutical analysis,[10,11] environment detection,[12,13] and food analysis.[14,15] However, to the best of our knowledge, few studies concerning the ECL immunoassay for detecting OTA have been reported. Thus, in this study, a sensitive ECL immunosensor based on $Au/CaCO_3$ for the OTA detection has been developed for the first time.

In the ECL systems, the luminescent probe of $Ru(bpy)_3^{2+}$ is commonly utilized for immunoassay owing to high light efficiency, excellent stability, good biocompatibility, and superior electrochemical properties.[16] Previously, the Nafion cation-exchange membrane method is usually used for immobilizing $Ru(bpy)_3^{2+}$.[17−19] However, this approach has some drawbacks, such as time-consuming, reagent-consuming, and luminescent reagent fixed easily falling off. In recent years, different nanomaterials is used as carriers in immobilizing $Ru(bpy)_3^{2+}$ to improve the ECL performance, for example, silica nanoparticles (SiO_2 NPs),[20−22] metal−organic frameworks (MOFs),[23−25] poly(amidoamine dendrimer) (PAMAM),[26,27] and metal nanomaterials.[28,29] Among these nanomaterials, unique metal nanomaterials using waste eggshells as a template to prepare a series of Ag/eggshell, Pt/eggshell, and Au/eggshell nanocomposites have attracted the attention of a lot of researchers. Compared with other precious metal nanoparticles, Au nanoparticles have special merits because of their high catalytic activity and excellent electrical conductivity.[30] Furthermore, using a waste eggshell as a carrier has typical merit because its porous hierarchical structure allows it to not only entrap Au ions well, preventing their aggregation, but also immobilize a large amount of $Ru(bpy)_3^{2+}$ to greatly increase the ECL signal. In addition, the $Au/CaCO_3$ nanocomposites possess high stability because the eggshell is quite stable after calcination, further improving the stability of ECL immunosensors. Importantly, exploring the research value of the waste, abundant, and low-cost eggshells and the change of waste into wealth would contribute tremendously to environmental remediation and socially sustainable development. Based on these considerations, we synthesize functional Au-nanoparticle-coated waste eggshell nanocomposites ($Au/CaCO_3$ nanocomposite) via a simple mixing and calcination strategy, which is used as an ideal ECL immunosensor platform for loading $Ru(bpy)_3^{2+}$.

With the rapid development of genetic engineering and phage display techniques, a particular class of antibodies, known as nanobodies (Nbs) derived from different regions of heavy chain antibody in camelids, has attracted the attention of researchers. Nbs have several apparent merits compared to conventional antibodies, such as smaller molecular weight (15 000), high solubility, high affinity, and high solubility expression in a microbial system.[31] Due to these unique properties, the increasing number of Nbs for the small molecule and harmful substances were isolated and utilized as the recognition elements in immunoassays. For example, Liu's group reported the research about Nb-based ELISA for OTA detection in cereals with strong resistance to matrix interference, which was attributed to the good tolerance of Nb28 to methanol.[32] Moreover, to further expand OTA Nb applications in immunoassay, Nbs are gene modifications to construct fusions protein with alkaline phosphatase and green fluorescence. For instance, Liu et al. reported the Nb-avitag fusion protein based on the ELISA approach for the OTA detection in cereals.[33] To the best of our best knowledge, there are no reports on the application of OTA Nbs in an ECL immunoassay. The integration of the OTA Nbs with the ECL method would lead to the development of an immunosensor with high sensitivity and specificity, solving the problem related to matrix interference of ECL immunosensors in food analysis.

Herein, a novel ECL immunosensor based on $Au/CaCO_3$ and OTA Nbs is fabricated for the sensitive detection of OTA. $Au/CaCO_3$ nanocomposites with a large surface area and high conductivity and stability are synthesized using waste eggshell as a template via economic and environmental-friendly transformation method. It is further applied for immobilizing $Ru(bpy)_3^{2+}$ due to the large pores and high conductivity, enhancing the sensitivity of the ECL immunosensor. Moreover, the prepared functional $Au/CaCO_3$ nanocomposites can provide active sites to conjugate with Nb via the Au−thiol bond. The constructed ECL immunosensor shows high

https://doi.org/10.1021/acsomega.1c05213
ACS Omega 2021, 6, 30148−30156

sensitivity for OTA with a linear range from 10 pg/mL to 100 ng/mL and a low detection limit of 5.7 pg/mL. Importantly, the proposed sensing interface with strong and stable ECL signals and high specificity could be successfully employed for the detection of OTA in the coffee sample with satisfactory performance.

2. RESULTS AND DISCUSSION

2.1. Characterization of Au/$CaCO_3$ Nanocomposites. The detailed morphology of Au/$CaCO_3$ composites was characterized by a scanning electron microscope (SEM) under different magnifications. As shown in Figure 1B, there are a large number of porous structures on the surface of Au/$CaCO_3$ composites to absorb more luminescent probes of $Ru(bpy)_3^{2+}$. Furthermore, it is clearly observed that a large amount of good AuNPs are uniformly immobilized on the surface of the eggshell (Figure 1C). The corresponding quantitative energy-dispersive X-ray spectrometer (EDS) mapping images of Au/$CaCO_3$ composites reveal that it is mainly composed of C, O, Au, and Ca (Figure 1D).

2.2. Expression, Purification, and Identification of Nb28. Nb28 was expressed by the auto-induction method and purified with a Ni-NTA sepharose column. The purification of Nb28 was characterized by sodium dodecyl sulfate-polyacrylamide gel electrophoresis (SDS-PAGE) and Western blot (Figure 2). An obvious target protein band of approximately

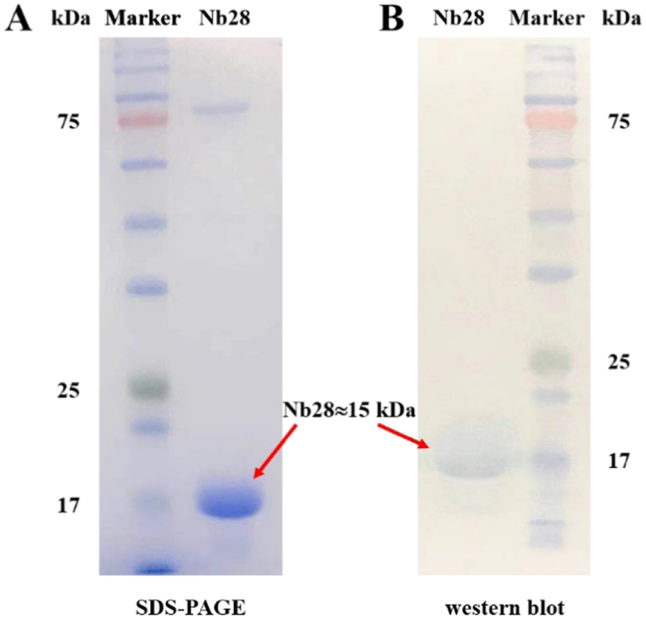

Figure 2. (A) SDS-PAGE gel stained with coomassie blue R250 and WB analysis of Nb28 (B).

15 kDa was observed by running SDS-PAGE (Figure 2A). The same bands were also obtained after WB using HRP-anti-His-Tag antibody as the probe (Figure 2B).

2.3. Electrochemical and Electrochemiluminescence Behaviors of the ECL Immunosensor. We use the cyclic voltammetry (CV) curve to characterize each step of the assembly of the modified electrode in Figure 3A. There is a pair of characteristic redox currents of $Ru(bpy)_3^{2+}$ in the 1 × phosphate-buffered saline (PBS) solution (curve a). Compared with that of $Ru(bpy)_3^{2+}$/Au/$CaCO_3$/Nafion/GCE, the characteristic redox currents of $Ru(bpy)_3^{2+}$ gradually decrease after the modification of Nb28 and BSA, which are attributed to the blocking effect of protein on interfacial electron transfer. After incubating the electrode with OTA, the CV signal strength continues to decrease due to the specific immune recognition reaction between nanobody and antigen. This result can explain the successful construction of the modified electrode. In addition, we also use electrochemical impedance spectroscopy (EIS) to verify the assembly step of the modified electrode (Figure S1 in the Supporting Information). Nafion greatly obstructs electron transfer due to its poor conductivity, thus increasing the EIS signal (curve b). In addition, $Ru(bpy)_3^{2+}$ could generate cation exchange with Nafion, leading to the production of abundant anions outside of the Nafion membrane, which increases the repulsive effect on the $[Fe(CN)_6]^{3-/4-}$ probe, resulting in the increase of the EIS value (curve c). After modifying BSA and OTA on the electrode, the blocking effect of protein (curve d) and the specific binding of antigen and antibody (curve e) can also reduce the electron transfer efficiency. Thus, the EIS signal increases. Besides, we investigate the effect of different scanning rates (50−300 mV/s) on the modified electrode in the 1 × PBS solution (Figure S2 in the Supporting Information). The peak current of CV is linearly related to the square root of the scanning rate in Figure S2B, which indicates that the electron transfer on the modified electrode surface is controlled by diffusion.

Furthermore, the ECL was applied to prove the construction process of the immunosensor (Figure 3B). The results are consistent with the variation of the CV curve (Figure 3A). As shown in Figure 3B, after the assembly of $Ru(bpy)_3^{2+}$/Au/$CaCO_3$/Nafion, the modified electrode (curve a) has a strong ECL signal strength in the 1 × PBS containing 0.05 mM TPA solution. However, when Nb28 and BSA are successively fixed on the electrode step by step, the ECL signal significantly decreases (curves b and c) because the proteins on the electrodes make electron transport less efficient, inhibiting the ECL reaction to form the excited-state $Ru(bpy)_3^{2+*}$. The reaction mechanism of ECL is based on the $Ru(bpy)_3^{2+}$/TPA system in Scheme 2.

In the scheme, first, TPA and $Ru(bpy)_3^{2+}$ are oxidized to produce TPA. and $Ru(bpy)_3^{3+}$ in the first step of the ECL reaction. The active radical of TPA. reacts with $Ru(bpy)_3^{3+}$ to generate the excited-state $Ru(bpy)_3^{2+*}$. The excited-state $Ru(bpy)_3^{2+*}$ is not stable and emits the maximum band at 620 nm of photons. After OTA is immobilized on the electrode (curve d), the ECL signal strength continues to decrease due to the specific immunological recognition reaction between Nb28 and OTA, which greatly blocked the electron transfer, resulting in a decrease in the number and rate of the excited-state $Ru(bpy)_3^{2+*}$. In summary, CV and ECL experiments show the successful formation of the ECL immunosensor.

2.4. Optimization of Analytical Conditions. In this work, the concentration and incubation time of Nb28 are studied to fabricate an immunosensor with excellent performance toward OTA determination. Moreover, Figure 4A displays the effects of different concentrations of Nb28 (5, 10, 15, 20, 25 μg/mL) on the ECL response in 0.05 mM TPA. The ECL signal is detected after the ECL immunosensor containing different concentrations of Nb28 is incubated with the same concentration of OTA (100 ng/mL). When the Nb28 concentration continues to increase, the specific binding of antigen and antibody increases along with the increase in impeding effect on electron transport, resulting in a continuous

https://doi.org/10.1021/acsomega.1c05213
ACS Omega 2021, 6, 30148−30156

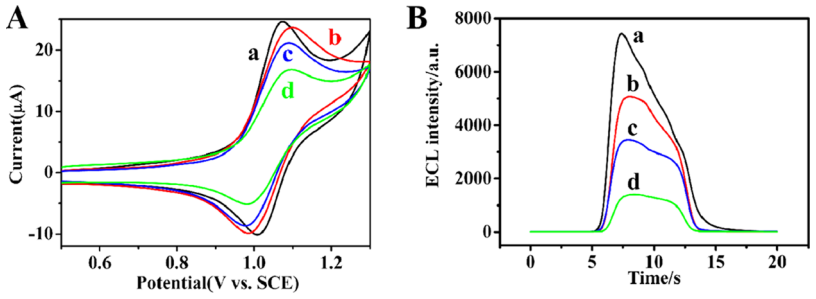

Figure 3. (A) CV curves in the 1 × PBS solution and (B) ECL responses in the 1 × PBS containing 0.05 mM Tris-*n*-propylamine (TPA) solution: (a) $Ru(bpy)_3^{2+}$/Au/$CaCO_3$/Nafion/GCE, (b) Nb28/$Ru(bpy)_3^{2+}$/Au/$CaCO_3$/Nafion/GCE, (c) BSA/ Nb28/$Ru(bpy)_3^{2+}$/Au/$CaCO_3$/Nafion/GCE, and (d) OTA/BSA/Nb28/$Ru(bpy)_3^{2+}$/Au/$CaCO_3$/Nafion/GCE. The voltage of the PMT was set at 600 V and the scan rate at 100 mV/s under the 3× magnification.

Scheme 1. Schematic Diagram of the Fabrication Process and Working Principle of the Nanobody-Based ECL

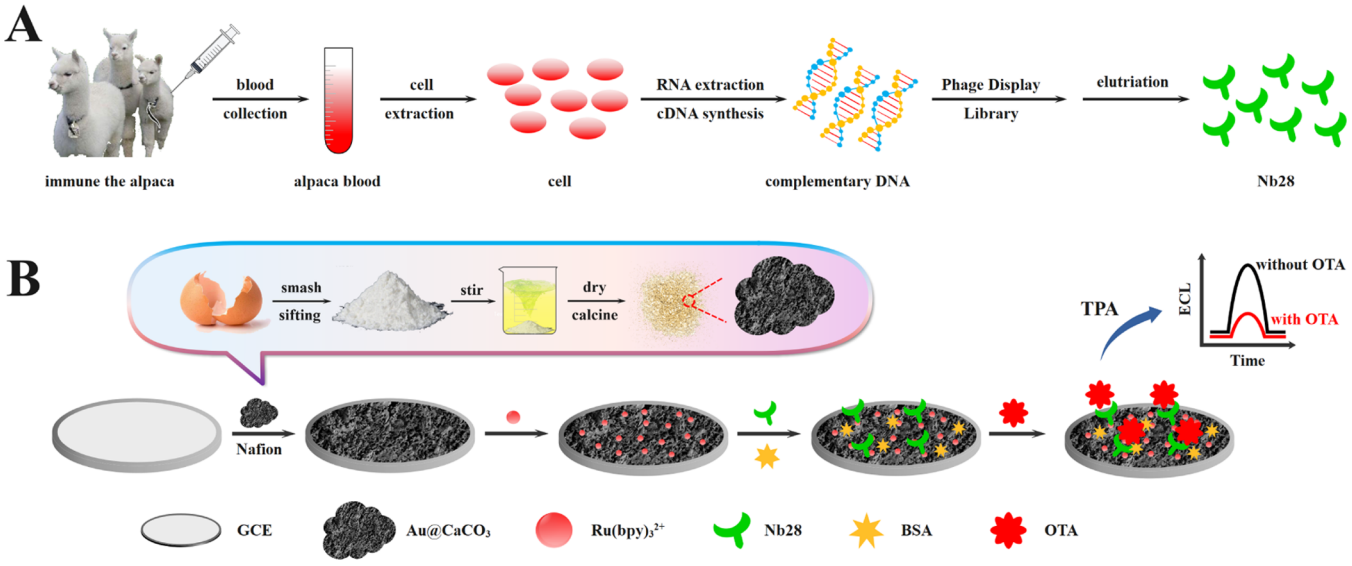

Scheme 2. Reaction Mechanism of ECL Sensor Based on the $Ru(bpy)_3^{2+}$/TPA System

$$Ru(bpy)_3^{2+} - e^- \rightarrow Ru(bpy)_3^{3+} \quad (1)$$

$$TPA - e^- \rightarrow TPA^{\cdot} + H^+ \quad (2)$$

$$TPA^{\cdot} + Ru(bpy)_3^{3+} \rightarrow Ru(bpy)_3^{2+*} \quad (3)$$

$$Ru(bpy)_3^{2+*} \rightarrow Ru(bpy)_3^{2+*} + \text{light (620 nm)} \quad (4)$$

decrease in the ECL signal. The ECL signal reaches a minimum of 20 μg/mL and achieves an equilibrium when the concentration continues to increase. Thus, the concentration of Nb28 of 20 μg/mL is employed in the following study. Afterward, the binding time of Nb28 is also significant for the OTA-specific recognition. As shown in Figure 4B, effects of binding time of Nb28 are also observed to range from 1 to 5 h. The results show that with the increase in the incubation time of Nb28, the ECL signal decreased obviously and reaches a plateau at 3 h when the time increases continuously. Thus, 3 h

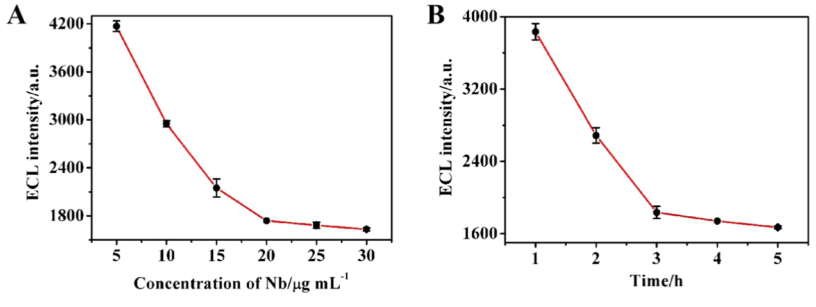

Figure 4. Effects of the concentration of Nb28 (A) and incubation time of Nb28 (B) on the ECL intensity in 1 × PBS containing 0.05 mM TPA. The voltage of the PMT was set at 600 V and the scan rate at 100 mV/s. The magnification is 3 times.

https://doi.org/10.1021/acsomega.1c05213
ACS Omega 2021, 6, 30148−30156

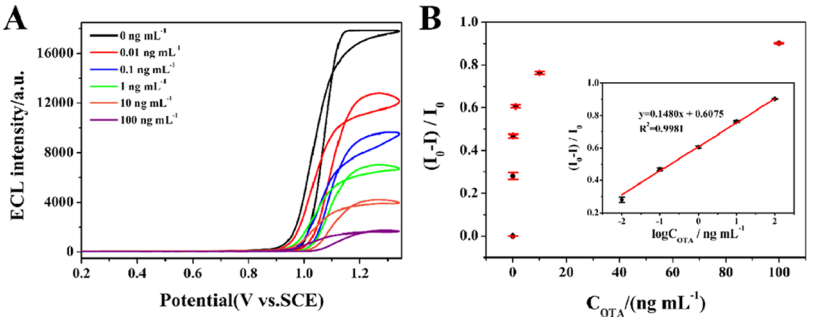

Figure 5. (A) Diagram of the ECL response versus the potential of the proposed immunosensor at different concentrations of OTA from 0.01 to l00 ng/mL in 1 × PBS containing 0.05 mM TPA solution. (B) Calibration curve of the ECL immunosensor for OTA detection. The voltage of the PMT was set at 600 V and the scan rate at 100 mV/s. The magnification is 4 times.

is considered the appropriate incubation time throughout the tests.

2.5. Quantitative Detection of OTA via the ECL Immunosensor. The ECL immunosensor prepared by the optimal conditions was used to detect OTA. As exhibited in Figure 5A, the luminescence signal gradually decreased with the increase in OTA concentration ranging from 0.01 to 100 ng/mL. With the increase in the OTA standard concentration, the number of specific immune binding of OTA antigens and antibodies was increased, inhibiting the electron transfer and thereby obstructing the ECL reaction and the ECL intensity. Accordingly, a good linear relationship between the inhibition ratio $(I_0-I)/I_0$ and the logarithm of OTA concentration is obtained in the range from 0.01 to 100 ng/mL with a low limit of detection (LOD) of 5.7 pg/mL (S/N = 3), which is lower than the maximum limit of 10 μg/kg in soluble coffee (European Commission). The linear regression equation was $(I_0-I)/I_0 = 0.1480 \log C_{OTA} + 0.6075$ with the correlation coefficient of $R^2 = 0.9981$.

Furthermore, the comparison between this sensor and the previously reported sensor for OTA detection is illustrated in Table 1. At present, the majority of the work using ECL sensors for OTA detection is based on molecularly imprinted polymer (MIP) as a recognition element. For example, Wang et al.[8,9] prepared a MIP-ECL sensor based on $Ru(bpy)_3^{2+}$-doped silica nanoparticles (RuSi-NPs), improving the selectivity and sensitivity of the sensor. Here, for the first time, we propose the novel ECL sensor for OTA detection using nanobodies as a recognition probe. The prepared sensor has a lower LOD and a wider linear range, suggesting that our fabricated ECL immunosensor could have extensive prospects in the application for an ultrasensitive OTA detection. The high sensitivity of the proposed ECL immunosensor could be attributed to the synergetic coupling of $Au/CaCO_3$ nanocomposites and Nb28. $Au/CaCO_3$ with pores could load a large amount of $Ru(bpy)_3^{2+}$ and offer sufficient electron conductivity and active capturing sites for assembling Nb28, improving the sensor's sensitivity.

Table 1. Comparison of the Analytical Parameters of Our Fabricated ECL Immunosensor with Reported Techniques for OTA Detection

measurement protocol	Linear range (ng/mL)	detection limit (pg/mL)	samples	refs
PEC[a]	0.001−10	0.51	maize	36
Co-ELASA[b]	0.001−1000	0.84	Groundnuts, coffee beans	7
EC[c]	0.1−1.0	80	malt	37
EC	0.5−20	96	coffee	38
Nb-FRET[d]	0.005−1	5	rice, barley, wheat, oats	39
ICA[e]	0.1−1.6	100	rice, corn, ginger, green bean	40
ECL	0.00001−11.13	0.003	corns, human serum	8
ECL	0.0001−14.76	0.027	corn	9
ECL	0.01−100	5.7	coffee	this work

[a]photoelectrochemical. [b]colorimetric enzyme-linked apta-sorbent assay. [c]electrochemistry. [d]nanobody (Nb)-mediated Förster resonance energy transfer (FRET) immunosensing. [e]immunochromatographic assay.

2.6. Stability, Specificity, and Repeatability of the ECL Immunosensor. Stability plays an crucial role in evaluating the ECL performance of the fabricated immunosensor. Thus, we investigated the stability of the ECL immunosensor at different OTA concentrations under optimal conditions. As depicted in Figure 6A, the relatively stable ECL curves at different concentrations of OTA are acquired under continuous cyclic potential scanning for 15 cycles. Additionally, the inset of Figure 6A displays that the relative standard deviation (RSD) of the ECL signal of the modified electrode containing 0.1 ng/mL OTA is only 3.63%, indicating that the ECL immunosensor has good stability to detect OTA. After storage in the refrigerator at 4 °C for 2 weeks, the ECL immunosensor retained 95.93% of its initial signal response, demonstrating that it had good long-term stability. A series of three replicate measurements from the batch were carried out to estimate the intra-assay reproducibility of the immunosensor, the result showed that the RSD is 3.25%, indicating that the acceptable repeatability of this immunosensor for OTA detection. For the purpose of assessing the selectivity of the constructed ECL immunosensor, it was incubated with several structurally similar toxins, including OTB, OTC, AFB1, ZEN, and DON under optimal conditions. As shown in Figure 6B, the ECL intensity of other toxins did not show an obvious decline compared with the blank. However, the ECL signal of the sensor significantly decreased after adding OTA. The test demonstrated that the constructed immunosensor had favorable selectivity for OTA detection.

2.7. Preliminary Analysis in Coffee Samples. Recovery tests were performed in coffee samples to assess the feasibility of our developed ECL immunosensor using the standard addition method. First, the suspension of coffee powder at a

https://doi.org/10.1021/acsomega.1c05213
ACS Omega 2021, 6, 30148−30156

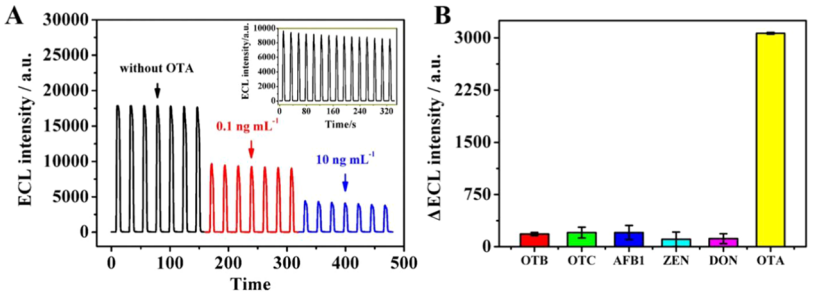

Figure 6. (A) ECL signal−time curve of the constructed ECL immunosensor in 1 × PBS with 0.05 mM TPA. (B) Specificity of the proposed ECL immunosensor incubated with the same concentration of OTA, OTB, OTC, AFB_1, ZEN, and DON (100 ng/mL) in 1 × PBS containing 0.05 mM TPA. The voltage of the PMT was set at 600 V and the scan rate at 100 mV/s.

concentration of 4 mg/mL was ultrasonicated for 30 min and then centrifuged to obtain the coffee supernatant. Different standard concentrations of OTA were added into the coffee supernatant so that different final concentrations of OTA in the coffee solution (0.05, 2, and 80 ng/mL) were acquired as the actual sample test solution. As displayed in Table 2, the

Table 2. Test Results of OTA in Coffee Samples

sample	added (ng/mL)	detected (ng/mL)	average (ng/mL)	recovery (%)	RSD (%)
1	0.05	0.047	0.05	99.56	6.23
		0.053			
		0.049			
2	2.00	2.03	2.03	101.32	5.12
		1.92			
		2.13			
3	80.00	79.80	80.94	101.17	1.34
		81.07			
		81.95			

acceptable RSD is no more than 6.23%, and the recoveries are 99.56, 101.32, and 101.17%, implying the promising analytical applications of the real coffee samples in the present ECL immunosensor.

3. CONCLUSIONS

In this work, a novel strategy of coupling Nb and $Au/CaCO_3$ nanocomposites was developed for constructing an ECL immunosensor to monitor OTA. $Au/CaCO_3$ nanocomposites were prepared by waste eggshells as the template, which not only had a large number of pores for loading more $Ru(bpy)_3^{2+}$ probe but also provided abundant binding sites (AuNPs) for the conjugation of Nb acting as a capture agent. As a result, the developed immunosensor exhibited good reproducibility, high stability, favorable specificity, and ultralow detection limit of OTA. Furthermore, the assay demonstrated that Nb28 with simplicity, good thermostability, and high affinity is a highly attractive candidate for the application of the ECL immunosensor. The study revealed that the proposed ECL immunosensor would provide a novel strategy for the sensitive determination of OTA in the coffee sample.

4. EXPERIMENTAL SECTION

4.1. Reagents and Materials. Absolute ethyl alcohol, KCl, $K_3Fe(CN)_6$, and $K_4Fe(CN)_6.3H_2O$ were all purchased from Aladdin Co. Ltd. (Shanghai, China). Bovine serum albumin (BSA) was ordered from Sigma Life Science Co. Ltd. (Shanghai, China). Chloroauric acid ($HAuCl_4$), Nafion perfluorinated resin solution (5 wt % in a mixture of lower aliphatic alcohols and water), and Tris(2,2′-bipyridyl) dichlororuthenium(II) hexahydrate were purchased from Sinopharm Chemical Reagent (Shanghai, China). Tri-*n*-propylamine (TPA) was received from Maclean Biotechnology Co., Ltd. (Shanghai, China). PBS (10 × 0.01 M, pH 7.2−7.4) and Ni-NTA sepharose were obtained from Solarbio Science & Technology Co., Ltd. (Beijing, China). OTA, OTB, OTC, Aflatoxin B_1 (AFB_1), zearalenone (ZEN), and deoxynivalenol (DON) were obtained from Pribolab Co., Ltd. (Qingdao, China). The vector Nb28-pET25b for Nb28 expression was previously prepared in our laboratory. The sample of coffee in this work was obtained from the supermarket in Haikou. The Millipore water purification system (18.2 MΩ/cm, Milli-Q) was used to prepare deionized water. All solutions used were prepared from deionized water, and all other reagents were analytical grade and used without further purification.

4.2. Apparatus. A model MPI-E electrochemiluminescence analyzer (Xi'An Remax Electronic Science & Technology Co. Ltd., Xi'an, China) was used to detect the ECL signal with the voltage of the photomultiplier tube (PMT) at 600 V. The cyclic voltammetry (CV) and electrochemical impedance spectroscopy (EIS) experiments were performed with the CHI660e electrochemistry workstation (Shanghai CH Instruments, China). A three-electrode system was used during the experiment consisting of a modified glass carbon electrode as a working electrode, a platinum wire as the auxiliary electrode, and an Ag/AgCl (3.5 M KCl) electrode as the reference electrode. Electrochemical impedance spectroscopy (EIS) experiments were performed with the CHI660e electrochemistry workstation (Shanghai CH Instruments, China) in 10 mM $[Fe(CN)_6]^{3-/4-}$ (1:1) containing 0.1 M KCl with the frequency range of 10^{-1} to 10^5 Hz. The $Au@CaCO_3$ nanocomposites' size and morphology were characterized by a scanning electron microscope (SEM) (Merlin Compact, ZEISS, Germany). Using energy-dispersive X-ray spectrometer (EDS) to detect the type of content and distribution of elements of $Au@CaCO_3$ nanocomposites.

4.3. Synthesis of $Au/CaCO_3$ Nanocomposites. Scheme 1B illustrates the synthetic process of the $Au/CaCO_3$ nanocomposites clearly.[34] First, waste eggshells from the canteen at the Hainan University were washed thoroughly with distilled water, the inner membrane was removed, then dried in an oven at 60 °C. The dried eggshells were ground into an ultrafine powder and passed through a 200-mesh sieve. Then, 1 g of ultrafine eggshell powder was added to 5 mL of 30% glacial acetic acid solution, mixed evenly, and soaked for 12 h. The acquired turbid liquid was subjected to a solid−

https://doi.org/10.1021/acsomega.1c05213
ACS Omega 2021, 6, 30148−30156

liquid separation, washed a few times, then dried in a vacuum oven at 60 °C to obtain the eggshell powder with a large number of pores. In this paper, the eggshell powder with pores was used as the template, and $HAuCl_4$ as the gold source to form composite material by the impregnation method at room temperature. Further, 0.5 g of eggshell powder with pores was added to the $HAuCl_4$ solution (0.1 M, 1 mL). The solution was stirred under a magnetic stirrer at room temperature and dried in an oven at 60 °C for 10 h. Finally, the obtained solid powder was placed in a crucible and calcined in a muffle furnace at 500 °C for 3 h at a heating rate of 2 °C per minute to get the $Au/CaCO_3$ nanocomposites.

$Au/CaCO_3$/Nafion was prepared as follows: 2 mg of synthesized $Au@CaCO_3$ nanocomposites was mixed with 1.3 mL of 2.5% Nafion solution at room temperature and shook vigorously for 2 h. Then, the above mixture was centrifuged at 10 000 rpm for 10 min to remove the excess Nafion. Subsequently, the resulting products were washed three times with deionized water. The final compounds were redispersed in 1 mL of deionized water and stored at 4 °C before use.

4.4. Preparation of Nb28. Before Nb28 expression, some processes such as alpaca immunization, library construction, and OTA-specific phage screening (Scheme 1A) were depicted according to the previous literature.[35] Moreover, Nb28 was expressed according to previous work with minor modifications. In brief, *Escherichia coli* BL21(DE3) cells containing the vector Nb28-pET25b were incubated in an auto-induction medium (100 mL) with ampicillin (100 μg/mL) at 37 °C by shaking at 250 rpm until the OD_{600} reached 0.5−0.7. The bacterial cells were continued to be cultivated at 25 °C by shaking at 200 rpm overnight for Nb28 auto-induction expression. After centrifugation, the cells in the culture were collected and suspended in 10 mL of PBS (0.01 M, pH 7.4). The resuspended cells were damaged by ultrasonic cell disruption and centrifuged at 10 000 rpm for 5 min. The supernatant containing the Nb28 proteins was filtered through a 0.22 μm sterile filter and then purified via a high-affinity protein purification column packed with Ni-NTA sepharose. After being dialyzed against PBS at 4 °C for 72 h, the purified Nbs were characterized by sodium dodecyl sulfate-polyacrylamide gel electrophoresis (SDS-PAGE) and Western blot (WB). The purity of Nbs was quantified by Nanodrop 2000, and Nbs were stored at −20 °C until use.

4.5. Fabrication of the ECL Immunosensor. Scheme 1B shows the step-by-step assembly and identification process of the prepared ECL immunosensor. Before modification, the GCE was polished with 0.3 and 0.05 μm alumina powder, then ultrasonicated with ethanol and distilled water for 2 min to obtain a mirror-like surface, and dried by nitrogen. Then, 5 μL of $Au/CaCO_3$/Nafion nanocomposites was dropped onto the pretreated surface of the electrode. After drying naturally in the air, the prepared $Au/CaCO_3$/Nafion/GCE electrode was immersed in 20 mM $Ru(bpy)_3^{2+}$ solution in the dark for 1 h. Thus, hydrophobic cation $Ru(bpy)_3^{2+}$ can be easily incorporated into the composite films composed of cation-exchangeable Nafion and $Au/CaCO_3$ nanocomposites via both an ion-exchange process and hydrophobic interactions. After rinsing with deionized water to wipe off the $Ru(bpy)_3^{2+}$ solution which was not adhered to the electrode surface, let it dry in a natural environment. According to the UV−vis spectra measurement, the $Ru(bpy)_3^{2+}$ content on the modified electrode was estimated to be 1.5×10^{-4} mg (Figure S4 in the Supporting Information). To attach the target molecules, 5 μL of Nb28 solution was coated on the surface of the $Ru(bpy)_3^{2+}/Au/CaCO_3$/Nafion/GCE, incubated at 37 °C for 3 h, and washed with distilled water to remove nonbound Nb28 molecules. In this process, thiol groups of Nb28 were conjugated with Au nanoparticles of $Au/CaCO_3$ via an Au−S bond. Subsequently, the modified electrode was incubated with 5 μL of the BSA solution (1%) at room temperature for 1 h to block nonspecific binding sites and then washed with distilled water gently. Finally, the obtained ECL immunosensor was stored at 4 °C until use.

■ ASSOCIATED CONTENT

Supporting Information

The Supporting Information is available free of charge at https://pubs.acs.org/doi/10.1021/acsomega.1c05213.

Nyquist plots of EIS of each step of the assembly of the modified electrode in 10 mM $[Fe(CN)_6]^{3-/4-}$ (1:1) containing 0.1 M KCl; CV curves of the modified electrode at different scan rates (50−300 mV/s) in 1 × PBS solution and a linear relationship between the square root of the scan rate and the current density; ECL responses of $Ru(bpy)_3^{2+}/CaCO_3$/GCE, $Ru(bpy)_3^{2+}$/Nafion/$CaCO_3$/GCE, $Ru(bpy)_3^{2+}/Au/CaCO_3$/GCE, and $Ru(bpy)_3^{2+}$/Nafion/$Au/CaCO_3$/GCE in 1 × PBS containing 0.05 mM TPA solution; and determination of $Au/CaCO_3$ and $Ru(bpy)_3^{2+}/Au/CaCO_3$ by UV−vis spectroscopy (PDF)

■ AUTHOR INFORMATION

Corresponding Authors

Hongmei Cao − *College of Food Science and Technology, Hainan University, Haikou 570228, China;* orcid.org/0000-0002-7044-5043; Email: hmcao@hainanu.edu.cn

Da-Peng Yang − *College of Chemical Engineering and Materials Science, Quanzhou Normal University, Quanzhou, Fujian Province 362000, China; School of Food Engineering, Ludong University, Yantai, Shandong 264025, China;* orcid.org/0000-0003-3509-2825; Email: yangdp@qztc.edu.cn

Authors

Linzhi Li − *College of Food Science and Technology, Hainan University, Haikou 570228, China*

Xing Liu − *College of Food Science and Technology, Hainan University, Haikou 570228, China;* orcid.org/0000-0002-1301-4837

Saijun He − *College of Food Science and Technology, Hainan University, Haikou 570228, China*

Benchao Su − *College of Food Science and Technology, Hainan University, Haikou 570228, China*

Tianzeng Huang − *College of Chemistry and Engineering Technology, Hainan University, Haikou 570228, China*

Qi Chen − *College of Food Science and Technology, Hainan University, Haikou 570228, China*

Minghuan Liu − *College of Chemical Engineering and Materials Science, Quanzhou Normal University, Quanzhou, Fujian Province 362000, China*

Complete contact information is available at: https://pubs.acs.org/10.1021/acsomega.1c05213

Author Contributions

[⊥]L.L. and X.L. contributed equally to this work.

Notes

The authors declare no competing financial interest.

■ ACKNOWLEDGMENTS

This work was supported by the Hainan Provincial Natural Science Foundation of China (320QN204, 2019RC129, and 2019RC119), the National Natural Science Foundation of China (31760493), and the Scientific Research Foundation of Hainan University (grant number KYQD(ZR)1939 and KYQD(ZR)1952).

■ REFERENCES

(1) Khataee, A.; Sohrabi, H.; Arbabzadeh, O.; Khaaki, P.; Majidi, M. R. Frontiers in conventional and nanomaterials based electrochemical sensing and biosensing approaches for Ochratoxin A analysis in foodstuffs: A review. *Food Chem. Toxicol.* **2021**, *149*, No. 112030.

(2) Quintela, S.; Villarán, M. C.; Armentia, I. L. D.; Elejalde, E. Ochratoxin A removal in wine: A review. *Food Control* **2013**, *30*, 439−445.

(3) Ventura, M.; Anaya, I.; Broto-Puig, F.; Agut, M.; Comellas, L. Two-dimensional thin-layer chromatographic method for the analysis of ochratoxin A in green coffee. *J. Food Prot.* **2005**, *68*, 1920−1922.

(4) Zareshahrabadi, Z.; Bahmyari, R.; Nouraei, H.; Khodadadi, H.; Mehryar, P.; Asadian, F.; Zomorodian, K. Detection of Aflatoxin and Ochratoxin A in Spices by High-Performance Liquid Chromatography. *J. Food Qual.* **2020**, *2020*, No. 8858889.

(5) Rodríguez-Carrasco, Y.; Font, G.; Manes, J.; Berrada, H. Determination of Mycotoxins in Bee Pollen by Gas Chromatography-Tandem Mass Spectrometry. *J. Agric. Food Chem.* **2013**, *61*, 1999−2005.

(6) Meerpoel, C.; Vidal, A.; di Mavungu, J. D.; Huybrechts, B.; Tangni, E. K.; Devreese, M.; Croubels, S.; De Saeger, S. D. Development and validation of an LC-MS/MS method for the simultaneous determination of citrinin and ochratoxin a in a variety of feed and foodstuffs. *J. Chromatogr. A* **2018**, *1580*, 100−109.

(7) Mukherjee, M.; Nandhini, C.; Bhatt, P. Colorimetric and chemiluminescence based enzyme linked apta-sorbent assay (ELASA) for ochratoxin A detection. *Spectrochim. Acta, Part A* **2021**, *244*, No. 118875.

(8) Wang, Q. L.; Chen, M. M.; Zhang, H. Q.; Wen, W.; Zhang, X. H.; Wang, S. F. Enhanced electrochemiluminescence of RuSi nanoparticles for ultrasensitive detection of ochratoxin A by energy transfer with CdTe quantum dots. *Biosens. Bioelectron.* **2016**, *79*, 561−567.

(9) Wang, Q. L.; Chen, M. M.; Zhang, H. Q.; Wen, W.; Zhang, X. H.; Wang, S. F. Solid-state electrochemiluminescence sensor based on RuSi nanoparticles combined with molecularly imprinted polymer for the determination of ochratoxin A. *Sens. Actuators, B* **2016**, *222*, 264−269.

(10) Li, Y. Y.; Wang, Y. G.; Liu, X. J.; Feng, R.; Zhang, N.; Fan, D. W.; Ding, C. F.; Zhao, H. Q.; Du, Y.; Wei, Q.; Ju, H. X. Bifunctional pd-decorated polysulfide nanoparticle of Co9S8 supported on graphene oxide: A new and efficient label-free immunosensor for amyloid *β*-protein detection. *Sens. Actuators, B* **2020**, *304*, No. 127413.

(11) Xue, J. W.; Yang, L.; Jia, Y.; Zhang, Y.; Wu, D.; Ma, H. M.; Hu, L. H.; Wei, Q.; Ju, H. X. Dual-quenching electrochemiluminescence resonance energy transfer system from Ru-In_2S_3 to α-MoO_3-Au based on protect of protein bioactivity for procalcitonin detection. *Biosens. Bioelectron.* **2019**, *142*, No. 111524.

(12) Wang, C.; Liu, L.; Liu, X. J.; Chen, Y.; Wang, X. Y.; Fan, D. W.; Kuang, X.; Sun, X.; Wei, Q.; Ju, H. X. Highly-sensitive electrochemiluminescence biosensor for NT-proBNP using MoS_2@Cu_2S as signal-enhancer and multinary nanocrystals loaded in mesoporous UiO-66-NH_2 as novel luminophore. *Sens. Actuators, B* **2020**, *307*, No. 127619.

(13) Nie, Y. X.; Zhang, X.; Zhang, Q.; Liang, Z. H.; Ma, Q.; Su, X. G. A novel high efficient electrochemiluminescence sensor based on reductive Cu(I) particles catalyzed Zn-doped MoS_2 QDs for HPV 16 DNA determination. *Biosens. Bioelectron.* **2020**, *160*, No. 112217.

(14) Cao, N.; Zhao, F. Q.; Zeng, B. Z. A novel ratiometric molecularly imprinted electrochemiluminescence sensor for sensitive and selective detection of sialic acid based on PEI-CdS quantum dots as anodic coreactant and cathodic luminophore. *Sens. Actuators, B* **2020**, *313*, No. 128042.

(15) Zhao, W. R.; Xu, Y. H.; Kang, T. F.; Zhang, X.; Liu, H.; Ming, A. J.; Cheng, S. Y.; Wei, F. Sandwich magnetically imprinted immunosensor for electrochemiluminescence ultrasensing diethylstilbestrol based on enhanced luminescence of Ru@SiO_2 by CdTe@ZnS quantum dots. *Biosens. Bioelectron.* **2020**, *155*, No. 112102.

(16) Li, J. X.; Shan, X. L.; Jiang, D.; Wang, W. C.; Chen, Z. D. An electrochemiluminescence aptasensor based on $Ru(bpy)_3^{2+}$ encapsulated titanium-MIL-125 metal-organic framework for bisphenol A assay. *Microchim. Acta* **2020**, *187*, 589−611.

(17) Xiong, X.; Zhang, P.; Lu, Y.; He, S.; Zhang, Y.; Jia, N. Q. A dual-signal electrochemiluminescence immunosensor based on $Ru(bpy)_3^{2+}$@3D-foam graphene and SnS_2 dots for sensitive detection of gastric cancer biomarker CA 72-4. *Talanta* **2021**, *221*, No. 121644.

(18) Zhang, R.; Zhong, X.; Chen, A. Y.; Liu, J. L.; Li, S. K.; Chai, Y. Q.; Zhuo, Y.; Yuan, R. Novel $Ru(bpy)_2(cpaphen)^{2+}$/TPrA/TiO_2 Ternary ECL System: An Efficient Platform for the Detection of Glutathione with Mn^{2+} as Substitute Target. *Anal. Chem.* **2019**, *91*, 3681−3686.

(19) Wang, H. M.; Wang, A. J.; Yuan, P. X.; Feng, J. J. Flower-like metal-organic framework microsphere as a novel enhanced ECL luminophore to construct the coreactant-free biosensor for ultrasensitive detection of breast cancer 1 gene. *Sens. Actuators, B* **2020**, *320*, No. 128395.

(20) Wu, B. N.; Hu, C. Y.; Hu, X. Q.; Cao, H. M.; Huang, C. S.; Shen, H. B.; Jia, N. Q. Sensitive ECL immunosensor for detection of retinol-binding protein based on double-assisted signal amplification strategy of multiwalled carbon nanotubes and $Ru(bpy)_3^{2+}$ doped mesoporous silica nanospheres. *Biosens. Bioelectron.* **2013**, *50*, 300−304.

(21) Liu, Q. L.; Bai, W. J.; Guo, Z. H.; Zheng, X. W. Enhanced electrochemiluminescence of $Ru(bpy)_3^{2+}$-doped silica nanoparticles by chitosan/Nafion shell@carbon nanotube core-modified electrode. *Luminescence* **2021**, *36*, 642−650.

(22) Li, L. B.; Chen, B. N.; Luo, L. J.; Liu, X. H.; Bi, X. Y.; You, T. Y. Sensitive and selective detection of Hg^{2+} in tap and canal water via self-enhanced ECL aptasensor based on NH_2-Ru@SiO^{2-}NGQDs. *Talanta* **2021**, *222*, No. 121579.

(23) Xiong, C. Y.; Liang, W. B.; Zheng, Y. N.; Zhuo, Y.; Chai, Y. Q.; Yuan, R. Ultrasensitive Assay for Telomerase Activity via Self-Enhanced Electrochemiluminescent Ruthenium Complex Doped Metal-Organic Frameworks with High Emission Efficiency. *Anal. Chem.* **2017**, *89*, 3222−3227.

(24) Qin, X. L.; Dong, Y. F.; Wang, M. H.; Zhu, Z. W.; Li, M. X.; Yang, D.; Shao, Y. H. In Situ Growing Triethanolamine-Functionalized Metal-Organic Frameworks on Two-Dimensional Carbon Nanosheets for Electrochemiluminescent Immunoassay. *ACS Sens.* **2019**, *4*, 2351−2357.

(25) Qin, X. L.; Zhang, X. H.; Wang, M. H.; Dong, Y. F.; Liu, J. J.; Zhu, Z. W.; Li, M. X.; Yang, D.; Shao, Y. H. Fabrication of Tris(bipyridine)ruthenium(II)-Functionalized Metal-Organic Framework Thin Films by Electrochemically Assisted Self-Assembly Technique for Electrochemiluminescent Immunoassay. *Anal. Chem.* **2018**, *90*, 11622−11628.

(26) Babamiri, B.; Hallaj, R.; Salimi, A. Ultrasensitive electrochemiluminescence immunoassay for simultaneous determination of CA125 and CA15-3 tumor markers based on PAMAM-sulfanilic acid-$Ru(bpy)_3^{2+}$ and PAMAM-CdTe@CdS nanocomposite. *Biosens. Bioelectron.* **2018**, *99*, 353−360.

https://doi.org/10.1021/acsomega.1c05213
ACS Omega 2021, 6, 30148−30156

(27) Jiang, W. J.; Wu, L. N.; Duan, J. L.; Yin, H. S.; Ai, S. Y. Ultrasensitive electrochemiluminescence immunosensor for 5-hydroxymethylcytosine detection based on Fe_3O_4@SiO_2 nanoparticles and PAMAM dendrimers. *Biosens. Bioelectron.* **2018**, *99*, 660−666.
(28) Huang, B. M.; Yao, C. W.; Zhang, Y. J.; Lu, X. Q. A novel label-free solid-state electrochemiluminescence sensor based on the resonance energy transfer from $Ru(bpy)_3^{2+}$ to GO for DNA hybridization detection. *Talanta* **2020**, *218*, No. 121126.
(29) Yan, Z. Y.; Wang, F.; Deng, P. Y.; Wang, Y.; Cai, K.; Chen, Y. H.; Wang, Z. H.; Liu, Y. Sensitive electrogenerated chemiluminescence biosensors for protein kinase activity analysis based on bimetallic catalysis signal amplification and recognition of Au and Pt loaded metal-organic frameworks nanocomposites. *Biosens. Bioelectron.* **2018**, *109*, 132−138.
(30) Luo, J.; Jiang, Y. N.; Guo, X. Y.; Ying, Y.; Wen, Y.; Lin, P.; Sun, Y.; Yang, H. F.; Wu, Y. P. SnO_2 nanofibers decorated with Au nanoparticles for $Ru(bpy)_3^{2+}$ sensitized photoelectrochemical determination of NO^{2-} in urine. *Sens. Actuators, B* **2020**, *309*, No. 127714.
(31) Maass, D. R.; Sepulveda, J.; Pernthaner, A.; Shoemaker, C. B. Alpaca (Lama pacos) as a convenient source of recombinant camelid heavy chain antibodies (VHHs). *J. Immunol. Methods* **2007**, *324*, 13−25.
(32) Liu, X.; Tang, Z. W.; Duan, Z. H.; He, Z. Y.; Shu, M.; Wang, X. X.; Gee, S. J.; Hammock, B. D.; Xu, Y. Nanobody-based enzyme immunoassay for ochratoxin A in cereal with high resistance to matrix interference. *Talanta* **2017**, *164*, 154−158.
(33) Sun, Z. C.; Lv, J. W.; Liu, X.; Tang, Z. W.; Wang, X. R.; Xu, Y.; Hammock, B. D. Development of a Nanobody-AviTag Fusion Protein and Its Application in a Streptavidin-Biotin-Amplified Enzyme-Linked Immunosorbent Assay for Ochratoxin A in Cereal. *Anal. Chem.* **2018**, *90*, 10628−10634.
(34) Ding, Q.; Kang, Z. W.; Cao, L. P.; Lin, M. S.; Lin, H. T.; Yang, D. P. Conversion of waste eggshell into difunctional Au/$CaCO_3$ nanocomposite for 4-Nitrophenol electrochemical detection and catalytic reduction. *Appl. Surf. Sci.* **2020**, *510*, No. 145526.
(35) Tang, Z. W.; Liu, X.; Wang, Y. Y.; Chen, Q.; Hammock, B. D.; Xu, Y. Nanobody-based fluorescence resonance energy transfer immunoassay for noncompetitive and simultaneous detection of ochratoxin a and ochratoxin B. *Environ. Pollut.* **2019**, *251*, 238−245.
(36) Wei, J.; Liu, S. Q.; Qileng, A.; Qin, W. W.; Liu, W. P.; Wang, K.; Liu, Y. J. A photoelectrochemical/colorimetric immunosensor for broad-spectrum detection of ochratoxins using bifunctional copper oxide nanoflowers. *Sens. Actuators, B* **2021**, *330*, No. 129380.
(37) Sun, C. N.; Liao, X. F.; Huang, P. X.; Shan, G. Z.; Ma, X.; Fu, L. Z.; Zhou, L. D.; Kong, W. J. A self-assembled electrochemical immunosensor for ultra-sensitive detection of ochratoxin A in medicinal and edible malt. *Food Chem.* **2020**, *315*, No. 126289.
(38) Kunene, K.; Weber, M.; Sabela, M.; Voiry, D.; Kanchi, S.; Bisetty, K.; Bechelany, M. Highly-efficient electrochemical label-free immunosensor for the detection of ochratoxin A in coffee samples. *Sens. Actuators, B* **2020**, *305*, No. 127438.
(39) Tang, Z. W.; Liu, X.; Su, B. C.; Chen, Q.; Cao, H. M.; Yun, Y. H.; Xu, Y.; Hammock, B. D. Ultrasensitive and rapid detection of ochratoxin A in agro-products by a nanobody-mediated FRET-based immunosensor. *J. Hazard. Mater.* **2020**, *387*, No. 121678.
(40) Bu, T.; Zhang, M.; Sun, X. Y.; Tian, Y. M.; Bai, F. E.; Jia, P.; Bai, Y. W.; Zhe, T. T.; Wang, L. Gold nanoparticles-functionalized microorganisms assisted construction of immunobiosensor for sensitive detection of ochratoxin A in food samples. *Sens. Actuators, B* **2019**, *299*, No. 126969.

https://doi.org/10.1021/acsomega.1c05213
ACS Omega 2021, 6, 30148−30156